Reactivity of Sulfur/Polysulfide in Carbon-Sulfur Composite Cathodes of Lithium-Sulfur Batteries

Journal:	*ACS Applied Materials & Interfaces*
Manuscript ID	am-2017-06660p
Manuscript Type:	Article
Date Submitted by the Author:	12-May-2017
Complete List of Authors:	Burgos, Juan C. ; Universidad de Cartagena, Physics; Texas A&M Engineering Balbuena, Perla; Texas A&M University, Department of Chemical Engineering Montoya, Javier; Universidad de Cartagena, Física

Reactivity of Sulfur/Polysulfide in Carbon-Sulfur Composite Cathodes of Lithium-Sulfur Batteries

Juan C. Burgos,[†,‡] Perla B. Balbuena,[*,‡] and Javier A. Montoya[*,†,¶]

†*Doctorado en Ciencias Físicas, Facultad de Ciencias Exactas y Naturales, Universidad de Cartagena, Cartagena, Colombia*

‡*Department of Chemical Engineering, Texas A&M University, College Station, Texas, USA*

¶*Instituto de Matemáticas Aplicadas, Universidad de Cartagena, Cartagena, Colombia*

E-mail: balbuena@tamu.edu; jmontoyam@unicartagena.edu.co

Abstract

Lithium-sulfur batteries are promising non-conventional sources of energy due to their high theoretical capacity and energy density. However, the successful implementation of this technology has been hindered due to the low cycling life of the battery, caused by long chain polysulfide shuttling between electrodes during charge/discharge, among other issues. Quantum chemical calculations are used to study the reactivity of sulfur in the porous cathode of lithium-sulfur batteries, and the retention capabilities of porous carbon materials to avoid long chain polysulfide diffusion. Ab initio molecular dynamics (AIMD) simulations are initially employed to evaluate sulfur reduction mechanisms and kinetics, and to identify main reduction products. A porous cathode architecture is modeled through parallel graphene layers with elemental sulfur rings in the interlayer, and filled with 1,3-dioxolane (DOL) organic solvent and lithium ions. AIMD simulations showed fast reduction of elemental sulfur and formation of short

chain polysulfide. Furthermore, the effect of dangling carbon bonds of graphene on the reactivity of the cathode was confirmed. Adsorption calculations through density functional theory (DFT) proved the capacity of small pores to retain long polysulfide chains. An analysis of the effect of the specific current on the chemical behavior of sulfur reveals an influence of current on the amount of sulfur utilization and practical specific capacity of the battery. This work illustrates the physical-chemical behavior of the sulfur/polysulfide in the porous cathode system at atomistic level.

Introduction

Lithium Sulfur Batteries (LSBs) are a promising addition to the next generation energy storage devices due to their attractive high theoretical specific capacity and energy density. Due to these outstanding properties generated by the use of sulfur in the cathode, LSBs envision a future in transportation applications, in contrast to Li-ion batteries which are appropriate for small electronic devices.[1–5] Complete reduction of elemental sulfur in cathodes yields a theoretical specific capacity of 1673 mAh/g, and an energy density of 2500 Wh/kg,[4] which is significantly larger than the corresponding values in graphite-based and some silicon-based cathodes.[3,4] In addition to the aforementioned technical advantages, the use of elemental sulfur in the cathode of LSBs also represents cost and environmental benefits due to the abundance of this element on the earth's crust.[5] However, Li-S systems are known for their complex and highly interconnected chemistry at the electrode surfaces and the liquid electrolyte medium. The solid sulfur cathode has specific issues including its low electronic and ionic conductivity and volumetric changes during lithiation and de-lithiation, which lead to swelling and pulverization.[3,4] In addition to the aforementioned issues, the longest polysulfide (PS) chains dissolve in the organic electrolyte solvents shuttling between the cathode and anode, taking the active material away from the cathode.[3–5] The insoluble polysulfide chains (Li_2S and Li_2S_2), conversely, precipitate on the cathode surface forming a passivating layer that makes the electrode electrochemically inaccessible resulting in capacity

fades due to mass losses.[3,6] Polysulfide shuttled from cathode to anode may result also in mass loss due to formation and deposition of insoluble sulfides on the anode surface.[5] The sum of all these issues results in lower specific energy densities compared to the theoretical, and specific capacity fades upon cycling.

Different approaches have been tried to overcome these technical limitations simultaneously, reaching outstanding performances with reversible capacities close to the theoretical and long cycling life.[3,4] For instance, nanostructured carbon/sulfur composite electrodes with specific structural designs provide a conductive surface for Li_2S and Li_2S_2 deposition, affording the consequential volumetric expansion. Their nanoporous architectures also act as a trapping network able to retain polysulfide dissolution into the electrolyte.[7,8] Graphene-oxide/sulfur composite materials have exhibited improved performances with stable capacities above 950 mAh/g and small decays per cycle in the first cycles.[9–11] This type of 2D oxide structures may anchor sulfide via strong interactions with oxide functional groups avoiding sulfur shuttle between electrodes. However, graphene-based electrodes do not always trap polysulfides efficiently, especially if the composite has an open structure unable to avoid polysulfide diffusing out of the cathode.[12] One-dimensional[13–15] and three-dimensional[16,17] architectures, such as carbon nanotube/sulfur and crossed-linked polymer/sulfur nanocomposites, have also exhibited improved reversible capacities and reduced capacity fade upon cycling. The high capacity retention was generally attributed to enhanced conductivity and ability to trap polysulfide by the novel carbon architectures. For the specific case of 3D structures, disulfide chemisorption to form polymer/sulfur cross-linked interconnections is also associated to the limited capacity decay in 3D architectures. Recently, it was reported the use of conductive 3D carbon compartments (CCs),[18] whose morphology with meso and macro-pores allows high sulfur loading and better contact between electrolyte and sulfur. Nevertheless, results from this multiscale computational and experimental study demonstrated that a sulfur loading and microstructure evolution must be carefully controlled in order to grant ionic transportation for better battery performance. This study also proved

the high reactivity originated at the edge sites of graphitic pores leading to fast reduction reactions and rapid formation of Li_2S/Li_2S_2 films. Despite the width of this multi-scale approach, some other phenomena remain to be studied in detail, such as of the kinetics of the sulfur reduction and identification of polysulfide species.

Although the innovation in materials employed in electrodes, and electrolyte solvents and additives has been remarkable, the capacity of experimental LSBs still fades upon cycling due to the issues described previously. The lack of understanding of many physical-chemical processes has not allowed developing a reliable device based on sulfur electrodes. The significant upgrades to the technology are yet not enough to satisfy transportation needs and start considering mass production of Li/S batteries. In order to address these limitations, density functional theory (DFT) and ab initio molecular dynamics (AIMD) simulations are used to elucidate reaction mechanisms, identify sulfur and polysulfide reduction products, and understand the role of porous-carbon materials on the cathode reactivity and PS dissolution. In this report, we will focus on 2D cathode structures based on materials with walls made of graphene. AIMD simulations will be performed at different pore sizes and sulfur content, and the reactivity of the systems will be analyzed through analysis of charge transfer and identification of different polysulfide species in their different anionic/molecular forms. From now on, any reference made along this manuscript to "$\mathbf{S}_n^{2-}$ **species**" will include all molecular (Li_2S_n) and anionic (LiS_n^{1-}, and S_n^{2-}) forms of S_n.

Computational methods

Ab initio molecular dynamics (AIMD) simulations of sulfur/carbon cathode systems are performed using the Viena ab initio simulation package (VASP).[19–22] AIMD simulations are carried out following the Born-Oppenheimer procedure[23,24] to describe the classical motion of ions, as implemented in VASP. The GGA-PBE[25,26] exchange correlation functional and the projector augmented wave (PAW)[27,28] pseudopotentials are used, with a plane wave en-

ergy cut-off of 400 eV. The time step is set to 1 femtosecond, and the systems are allowed to run enough time until most of the sulfur has been reduced to short polysulfide (PS) chains or the PS species have been stabilized without experiencing additional reduction. This time corresponds to ∼8 ps to guarantee the polysulfide chain becoming chemically stable within the system. Parrinello-Rahman dynamics[29,30] at constant pressure and temperature (NpT) is chosen in order to account for possible volume expansions due to polysulfide reduction. The temperature is set at 330 K using the Langevin thermostat,[31,32] and all Langevin friction coefficients for relevant atoms present in the organic solvent (C, O, H) are set at 5.0 ps^{-1}. The friction coefficient and the fictitious mass for Parrinello-Rahman lattice degrees of freedom are set at 5.0 ps^{-1} and of 20 amu, respectively. The convergence criterion for the electronic self-consistent loop performed each dynamic step is fixed to $1x10^{-4}$, whereas a 1x3x1 Monkhorst-Pack grid[33] is used for the Brillouin zone integrations carried out over the system. The partial occupancies are set to each orbital following the Gaussian smearing[34] method with a smearing width of 0.05 eV. Van der Waals corrections to the Kohn-Sham DFT energy are included through the DFT-D3 method method of Grimme with Becke-Jonson damping.[35,36] The same methods and parameters used for AIMD are employed for DFT optimizations, with the exception of statistical and dynamic variables such as time step, ensemble, temperature and thermostat. The ionic relaxations are computed thorough the conjugate-gradient algorithm.

The systems are designed to represent a porous graphitic cathode with two sulfur rings (S_8) at the edge of the pore. The pore is built by placing finite parallel graphene layers on the yz-plane at the bottom of an orthorhombic cell (Figure 1). The sulfur rings are located in such a way that their normal vectors are parallel to the y lattice vector and perpendicular to the normal vector of the graphene plane. The length of the z lattice vector is 22 Å, while the dimensions of the x and y lattice vectors are 20 and 7.32 Å, respectively. The high reactivity expected from the system guarantees the sulfur ring reduction into polysulfides to take place before a ring rotation does. This makes the system design and dimension of the y lattice

vector suitable to avoid undesirable sulfur-sulfur repulsions in the periodic system. The free volume is filled with organic solvent dioxolane (DOL) according to the reported density of this solvent (1.06 g/cm^3), and 16 Li atoms, which represents a lithium concentration of 0.013 mol/cm^3. The Li atoms added to random intermolecular spaces in the organic solvent represent the stoichiometric amount to make one of the two sulfur rings reduce from S_8 to S^{2-} species. When Li atoms are added to the solvent, there is an instantaneous charge transfer from the atoms to the solvent molecules that become slightly negatively charged, whereas the Li atoms become ions. The procedure is introduced to represent the excess of electrons that would be present in the cathode during discharge, causing the reduction of S atoms that is discussed in the following sections. The size of the pore is fixed by placing either one or two graphene layers at the bottom of the yz-plane, which results in pore sizes of 2 nm or 1 nm, respectively. DFT adsorption calculations are performed on polysulfide molecules placed in the middle of two parallel graphene layers with different separations.

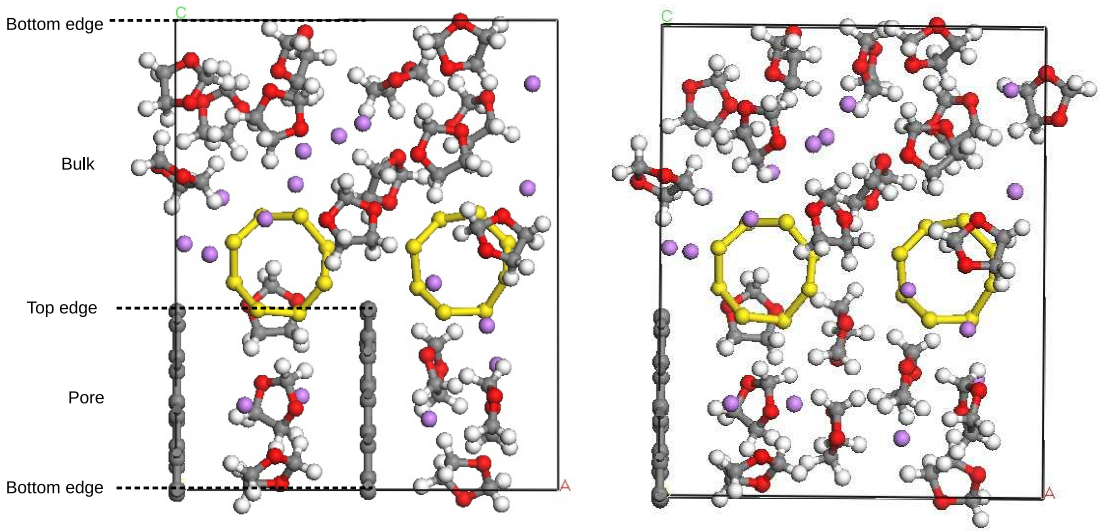

(a) (b)

Figure 1: Initial configuration of AIMD simulation cells. Sulfur is represented by yellow spheres, carbon is grey, lithium is purple, oxygen is red, and hydrogen is white. (a) Interlayer separation of 1 nm and a sulfur wt% of 44.2%. (b) Interlayer separation of 2 nm and S wt% of 61.3%

Results and discussion

Sulfur reduction and speciation

As explained above, the initial configuration has 16 Li atoms in the system that create a reactive environment despite being capable of reducing half of the total amount of sulfur to Li_2S. So, we expect the dynamics simulations to provide some insights into the kinetics of this process. AIMD simulations demonstrate that the system is very reactive and the first S^{2-} species start forming as early as before the first picosecond (blue line in Figures 2a and 2b). The presence of sulfide species (Li_2S, LiS^{1-}, and/or S^{2-}) might be an indicative of complete sulfur reduction. However, the observed rupture of S-S bonds in early stages of simulation does not strictly occur according to the sequential path that has been extensively reported ($S_8 \rightarrow Li_2S_8 \rightarrow Li_2S_6 \rightarrow Li_2S_4 \rightarrow Li_2S_2 \rightarrow Li_2S$).[3,4,37] On the contrary, our AIMD simulations showed that a S_2^{2-} can be produced before a S_6^{2-}, and species such as S_3^{2-} tend to form by quick reduction from S_8 and survive the highly reactive environment for long times of simulation, regardless of the pore size (Figure 2). The presence of S_5^{2-} and S_3^{2-} species in their anionic and radical anion forms are also in agreement with experimental evidence.[38] It is important to remark that S^{2-} and S_2^{2-} are formed quickly despite the fact that the amount of Li atoms (16) added was the stoichiometric amount needed for complete reduction of only one of the two sulfur rings in the system. Figure 2 illustrates also the effect of the pore size on the reaction. As we discussed earlier,[18] undercoordinated C atoms at the pore edges may facilitate the reduction. Figure 2 certainly show differences in the speciation between the 1 vs. 2 nm pores. All the larger species (S_6^{2-} and S_8^{2-}) are reduced immediately. For the S_n (with $n < 4$), we observe a difference between the 1nm and the 2nm pores: the smaller one tend to favor Li_2S whereas both Li_2S and Li_2S_2 are observed in the slightly larger pore. In both cases the presence of S_3^{2-} species is detected at the end of the simulation. Lithium ions are oxidized as a result of a charge transfer towards sulfur and two-coordinated carbon atoms at the pore's edge (Figure 3). An analysis of charges following the

Bader's Quantum Theory of Atoms in Molecules[39] demonstrates that large negative charges accumulate at the S ends of the polysulfide anions (Figure 3a), whereas the two-coordinated sulfur atoms in the inner part of polysulfide are less affected. As the length of the polysulfide becomes shorter, the charges of the two sulfur atoms at the chain-ends increase, as result of the sulfur-sulfur bond breaking leading to a net charge of $2e^-$ distributed along a shorter polysulfide. The high concentration of S^{2-} and S_2^{2-} species stabilized in the presence of low lithium concentration suggests the formation of polysulfide in stable anionic forms (LiS_n^{1-} and S_n^{2-}), which is confirmed by the ionic concentration profile for S_3^{2-} species in the figure 4a. The detail of the distribution of ionic polysulfide species (Figure 4) is recognized from the quantification of charges of individual atoms, which are added up for polysufide chains, and from the evaluation of S-Li interatomic distances. A significant difference between figures 2a and 2b lies on the concentration of S_4^{2-} species, which provides some preliminary insights about the effect of the pore size on the reactivity of the cathode. At least one S_4^{2-} chain remains in the reactive environment, only when the pore size is 1 nm. The trajectory frame in the figure 3a illustrates that the S_4^{2-} chain is located between the two graphitic layers of the pore, trapped without being able to diffuse or react. The concentration profile in figure 2a confirms the presence of S_4^{2-} in any of its molecular (Li_2S_4) or anionic configurations (LiS_4^{1-} and S_4^{2-}) for at least 2.6 ps. Figure 4b shows that the subsistence of S_4^{2-} is extended to times up to 8 ps, proving its stability in the graphitic confined system. Figure 4b also proves that the S_4^{2-} species is mostly seen in its molecular form (Li_2S_4), rather than any of the anionic states.

Two possible factors may explain the prolonged presence of S_4^{2-} inside the pore. As seen in figures 3 and 5, and also reported elsewhere,[18] the pore edge is a region of high reactivity where the Li ions tend to accumulate and sulfur reductions normally take place. Therefore, Li ions see their diffusivity into the pore hindered due to strong interactions with the pore edge. A Bader charge analysis demonstrates the significant reduction undergone by the edge atoms in the graphene, which is the evidence of strong Li-C interaction nearby that specific

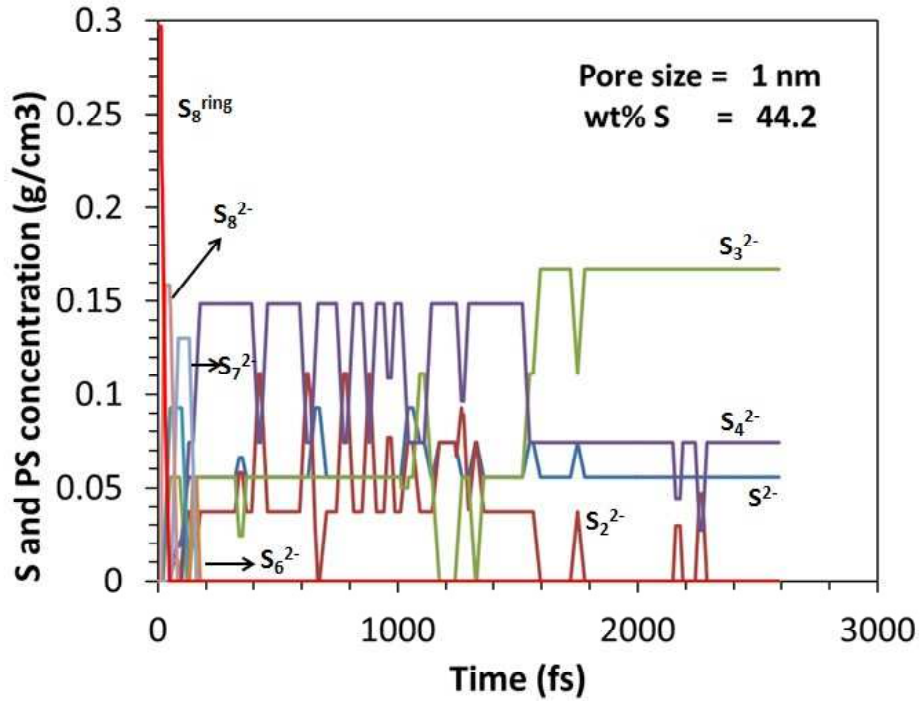

(a)

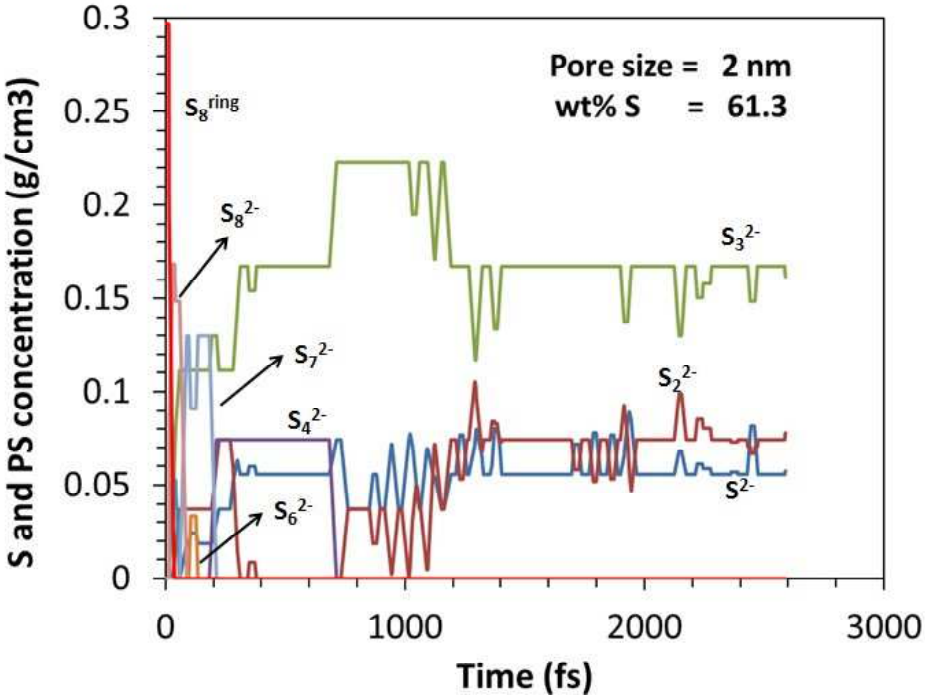

(b)

Figure 2: Concentration profile of polysulfide species along the AIMD trajectory. The concentrations are labeled as S_n^{2-} but that not necessarily means they are in that anionic form. The concentrations correspond to the sum of anionic and molecular forms of an specific S_n species. (a) Interlayer separation of 1 nm. (b) Interlayer separation of 2 nm.

area (Figure 3b). In our previous report,[18] it was shown from AIMD simulations and Z density profile analysis, that Li ions accumulate nearby the pore edge. A similar z-density profile of Li ions is also reported here (figure 5). In addition to spotting Li ions just outside the pore, two small peaks below the 8 Å mark indicate the presence of Li ions inside the pore. These two seem to be attached to the S_4^{2-} anion chain ends to form a Li_2S_4, as seen from the peaks separation of 4 Å (between 3 and 7 Å). However, these Li ions will hardly induce further reduction of the S_4^{2-} as the Li_2S_4 molecule becomes stable trapped between grephene walls, as shown in the S_4^{2-} species concentration profile in figure 4b. Besides those two to trapped Li ions forming a polysulfide molecule, no further Li is seen inside the pore that may cause polysulfide splitting into shorter chains.

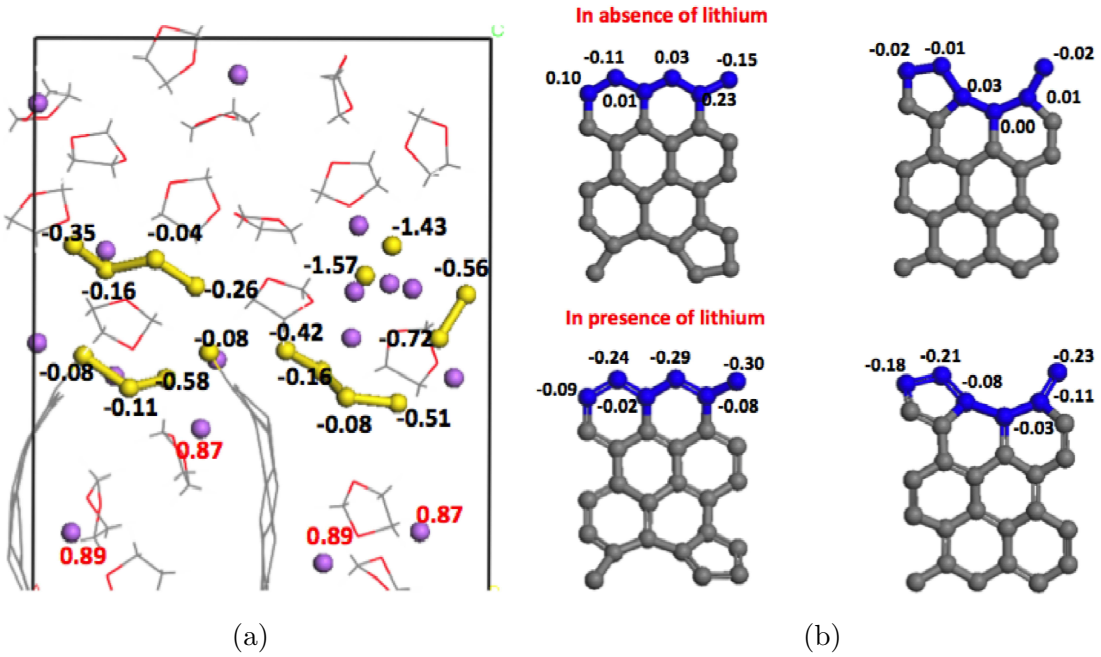

(a) (b)

Figure 3: (a) Charges of the sulfur and lithium atoms in solution. Red charge values correspond to lithium and black charge values to sulfur. (b) Charges of carbon atoms at the edge (blue atoms) of the graphene

On the other hand, the second factor is related to the restriction of the Li_2S_4 molecule to diffuse from inside the pore to the pore edge where the graphene dangling bonds create an area of high Li accumulation and high reactivity. As discussed above, porous materials might be able to trap polysulfide, diminishing their diffusion into the electrolyte solution, and

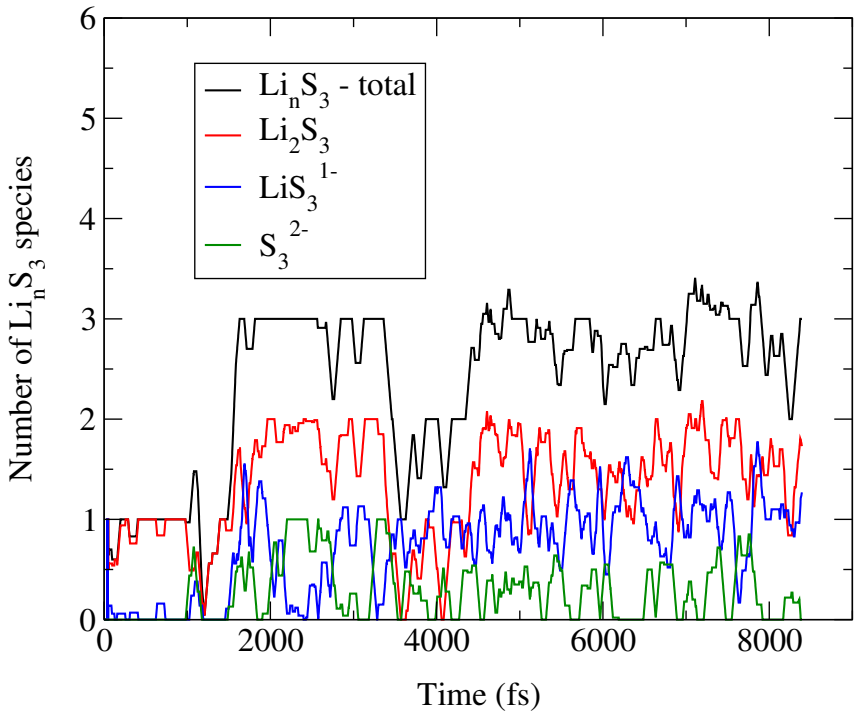

(a)

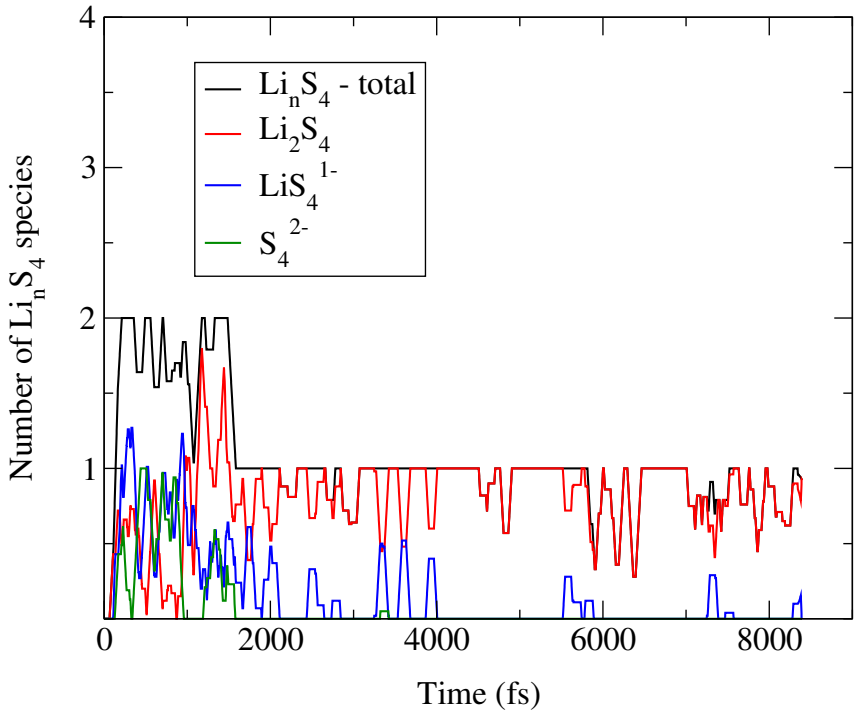

(b)

Figure 4: Concentration of (a) Li_nS_3 and (b) Li_nS_4 species in the 1 nm pore system. The black line corresponds to the sum of all the other curves. The almost perfect overlap of the black and red curves in the (b) graph demonstrates that the S_4 stabilizes in its molecular form (Li_2S_4).

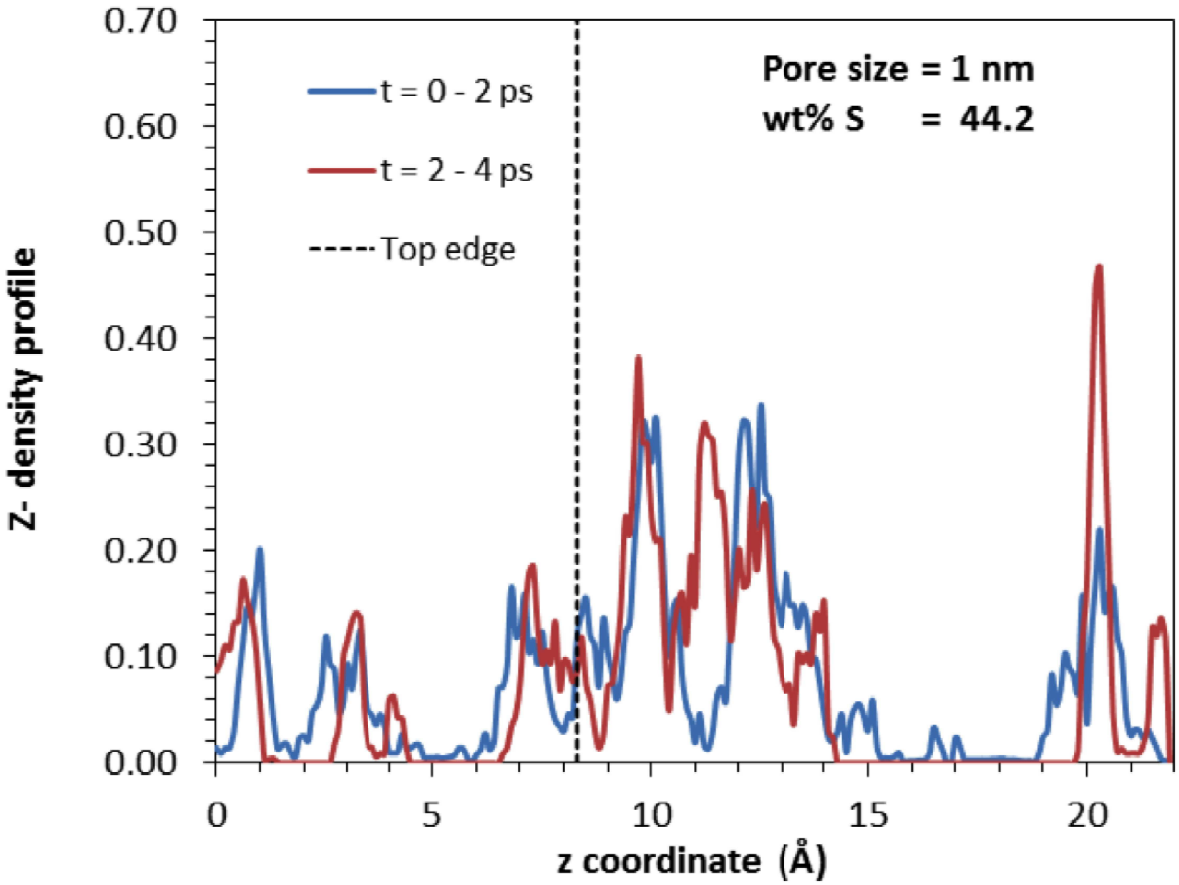

Figure 5: Z-density profile for Li ions in the system. Z-density profile for two time ranges (0 2 ps, and 2 to 4 ps). Li ions accumulate around the pore edges (dashed line, z=0, and z=22 Å). Two peaks inside the pore (z=3 and z=7 Å, approximately) indicating Li forming a Li_2S_4 molecule

consequently avoiding shuttling and improving battery performance. A limited diffusivity of the Li_2S_4 molecule is generally associated to strong adsorption interaction between the Li_2S_4 and the graphene surface. This interaction varies depending on the length of polysulfide chain and pore size (graphene layers separation). Figure 6 shows the result of DFT calculations on the polysulfide interaction with graphitic walls. The adsorption profiles show how the interaction becomes stronger as the pore size decreases and the sulfur chain length increases, from which we can infer that porous materials have a remarkable potential to act as a trap and retain polysulfide species near the cathode. Which is in agreement with some previous theoretical and experimental findings for carbon-based cathodes.[7,8,40] However, electrolyte solution or the organic solvent may potentially screen this PS/graphene adsorption and further investigation must be conducted in this direction.

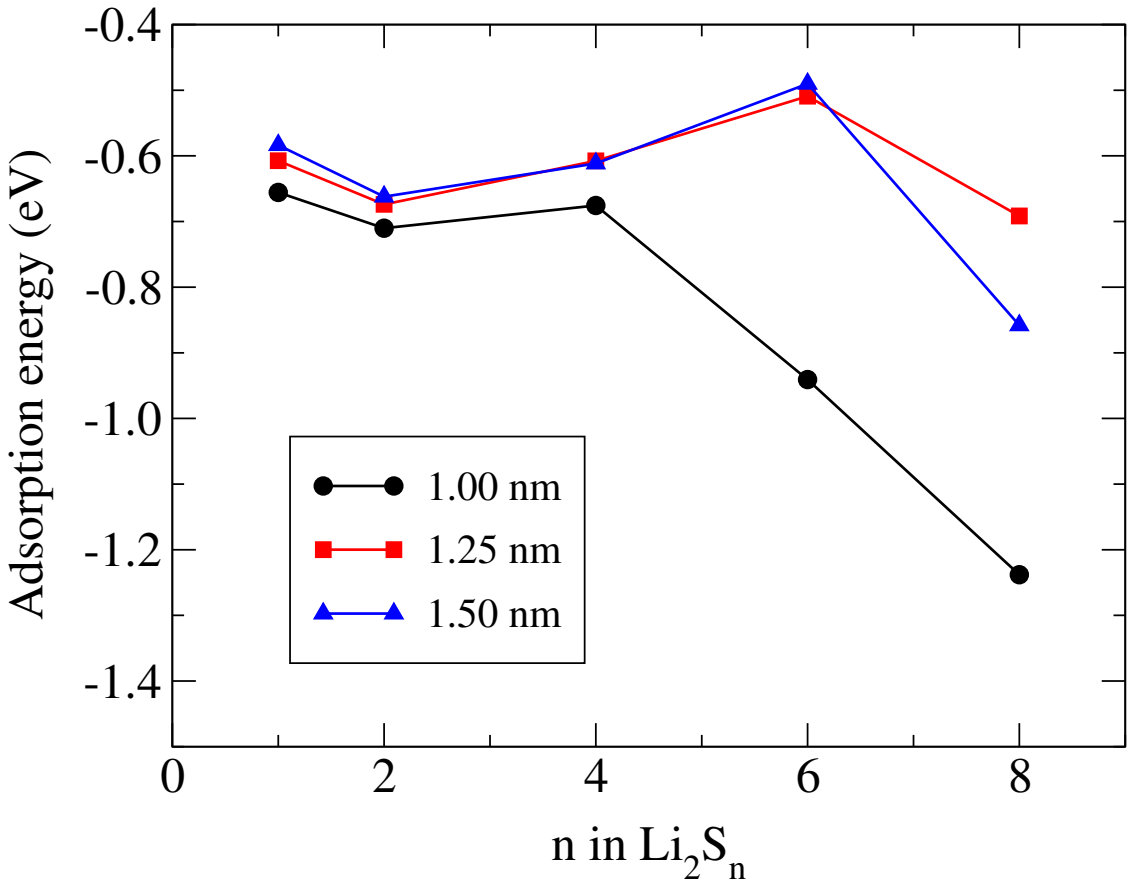

Figure 6: Adsorption energies of polysulfides as function of chain length and pore size

Effect of current on sulfur reduction mechanisms

In the previous section, the reactivity of the cathode was studied through the addition of a fixed amount of lithium into the simulation box, which was enough to convert half sulfur to Li_2S. In order to evaluate the effect of the lithium and electronic current on the reduction kinetics, a computational procedure consisting in sequential additions of lithium atoms is designed. The initial configuration of the system is redefined to have a 2 nm pore and only one sulfur ring in a system of same dimensions as the previous one (Figure 7). Two lithium atoms are then added sequentially in intervals of 100, 200, 300, and 400 fs until reaching 16 atoms in the simulation box, the stoichiometric amount to reduce all sulfur to Li_2S. As described above, the lithium atoms undergo an immediate charge transfer to the solvent and sulfur atoms to become Li ions. The Faraday's law relates the theoretical specific capacity (Q) to the number of electrons transferred to the host material (n) through the expression $Q = nF/M_r$, where F is the Faraday constant and M_r the molecular weight of the host material. Therefore, each two Li atoms added and ionized in the system are associated to an practical specific capacity as long as those electrons are transferred to the sulfur (a lithium-sulfur bond is formed). When the system reaches 16 Li atoms, it is allowed to run for the time interval corresponding to specific current, with no further Li addition. After 16 Li atoms have been added, the hypothetical reaction of all Li in the system into Li_2S results in a practical specific capacity matching the theoretical specific capacity calculated from the Faraday's law (1672.08 mAh g^{-1})

The total number of Li-S bonds formed during the simulation can be computed based on the evaluation of interatomic distances, in order to account for sulfur utilization. Figure 8 shows the profile of the total number of Li-S bonds as function of the percentage of elapsed time of simulation. The ideal sulfur reduction reaction implies that two lithium ions added to the system eventually form two Li-S bonds facilitating a $2e^-$ charge transfer to the host material, and an S-S bond breaking. This ideal scenario is represented by the horizontal dashed lines in the figure 8 that define both, the maximum number of Li-S bonds (left y-

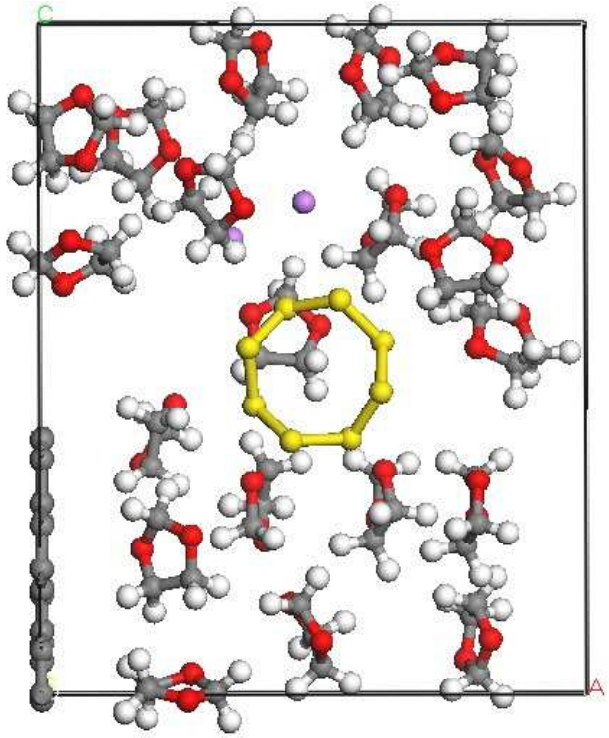

Figure 7: Initial configuration of AIMD simulation cells for current analysis. Sulfur is represented by yellow spheres, carbon is grey, lithium is purple, oxygen is red, and hydrogen is white. The interlayer separation is 2 nm and the sulfur wt% is 44.2%.

axis), and the corresponding maximum specific capacity value (right y-axis) for the amount of Li in the system. The complete reduction of the sulfur ring (S_8) to Li_2S means that 16 Li-S bonds have been formed after a total of 16 Li atoms have been added, and the practical theoretical capacity (1672.08 mAh g^{-1}) has been reached. However, this is not seen from our AIMD trajectories and the number of Li-S bonds is below 16 at the end of the simulations, regardless the rate of lithium supply. At low concentration of lithium in the system (at $\approx$ 35 % of elapsed time), the total number of Li-S bonds is observed to overcome the maximum amount of Li-S bonds that can be formed with the amount of Li atoms in the system (Figure 8c). This behavior is only seen for the current of 0.0067 e^-/fs, and it is expected from a calculation based on interatomic distances. Despite the high reactivity of the system, at very early stages of simulation the sulfur ring has not been fully reduced and sulfur atoms are held together through covalent bonds. Any approaching lithium ion will have a high probability of reaching bonding distances with more than one sulfur, until S-S bonds start breaking and polysulfide disperse in the electrolyte. Li-S bonds rapidly return below the maximum allowed (or ideal) as a result of dispersion and stabilization of newly formed polysulfide. Nevertheless, this behavior provides qualitative insights about the effect of the lithium current on the reactivity of sulfur and polysulfides. Slow supply of Li atoms into the system allows maximizing the number of Li-S bonds formed at early stages, as seen from the behavior of the blue lines in figures 8c and 8d frequently matching the maximum number of Li-S bonds (black dashed line) at times between 25 and 37.5%. Despite the chemical behavior of the system starts deviating from ideality after 64% of the simulation time has elapsed, the two lowest rates of charge supply still induce formation of a number of Li-S bonds closer to the ideal (16) by the end of the sequential addition of lithium atoms. Specific capacities in the order of 1200 mAh g^{-1} were reached near the end of simulation only for slow sequential addition of lithium (Figures 8c and 8d), whereas the highest rate of lithium addition yielded a specific capacity that did not overcome 1000 mAh g^{-1}, as seen in figure 8a. These results suggest that employing a low rate of lithium addition, or current, favor a higher

percentage of sulfur utilization, and therefore, a higher practical specific capacity, which is in agreement with experimental evidence.[18] A lower specific current allows lithium and sulfur finding minimal energy paths for reaction before the system is perturbed by introducing new Li atoms. Providing enough time between lithium supplies permits lithium to diffuse freely through the electrolyte seeking sulfur to induce S-S bond breaking.

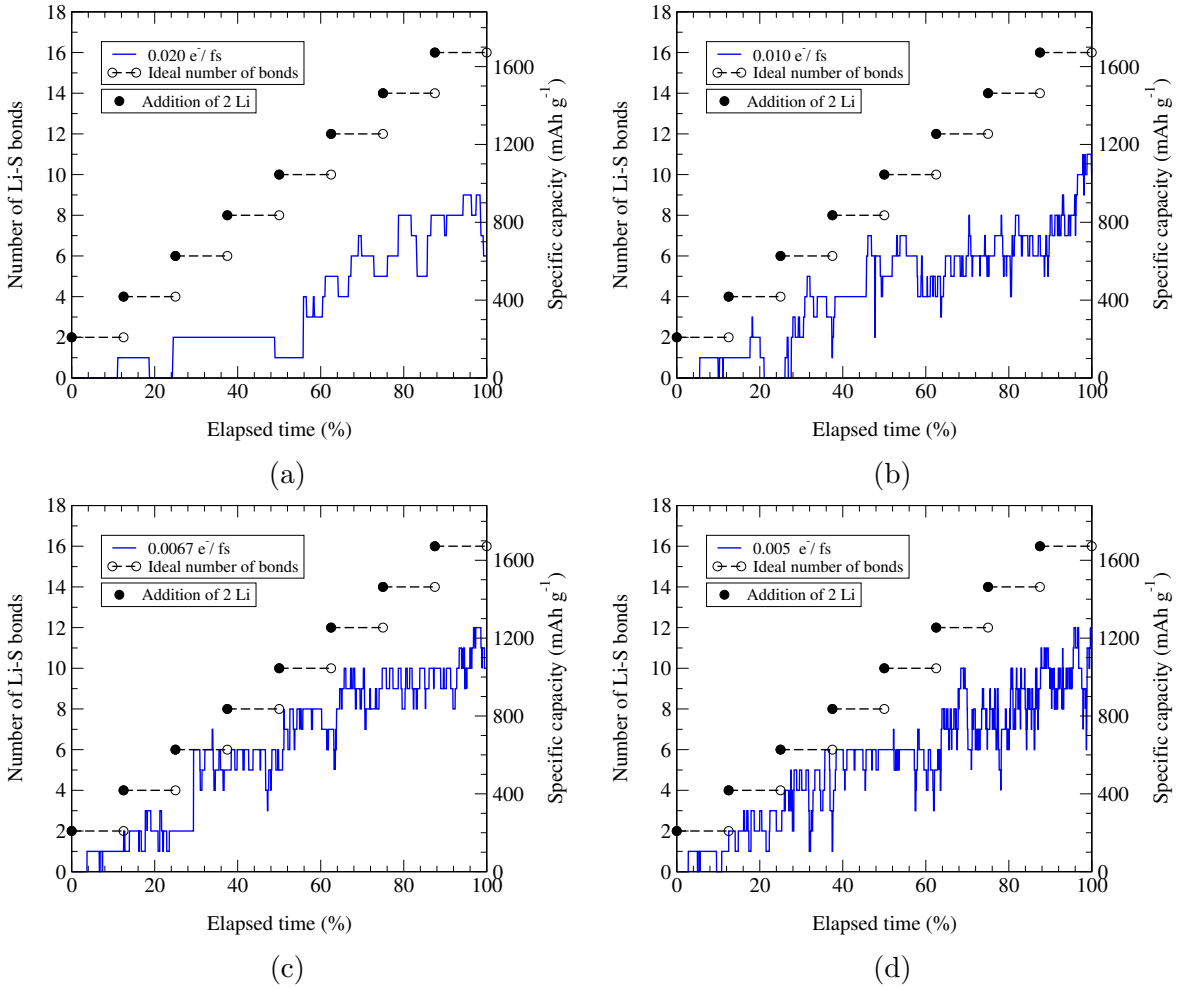

Figure 8: Number of Li-S bonds as function of the percentage of elapsed time and rate of addition of Li atoms into the system for (a) 0.020 e^-/fs, (b) 0.010 e^-/fs, (c) 0.0067 e^-/fs, and (d) 0.005 e^-/fs. The step function (black dashed lines) indicates the ideal number of Li-S bonds that should be reached according to the amount of Li in the system. The black dots indicate the exact instant at which a pair of Li atoms have been supplied.

A larger number of Li-S bonds can be translated into large concentrations of short poly-sulfide chains. This is confirmed by the concentration profiles in the figure 9. Figure 9a

shows that the lowest Li current used in this study leads to the high concentration of S^{2-} species. Conversely, the concentration profile of sulfur/polysulfide species for the highest Li current (Figure 9b) exhibits a high concentration of S_2^{2-} species after all Li have been supplied, which supports what is claimed from the analysis of Li-S bonds: Low Li currents favor higher sulfur utilization and specific capacities. Lithium current certainly affects the sulfur reduction mechanisms as inferred from a comparison of figures 9a and 9b. According to the figure 9a, low Li currents favor direct formations of short polysulfides from long polysulfide. For instance, reaction paths such as $S_6^{2-} \rightarrow S_2^{2-} + S_4^{2-}$ or $S_4^{2-} \rightarrow S^{2-} + S_3^{2-}$ are identified from the concentration profiles in figure 9a. It is also seen from the figure 9a that at initial stages of the sequential addition of Li (time $< 20\%$), the reaction path $S_8^{2-} \rightarrow S_7^{2-} + S^{2-}$ seems to take place. However, S_7^{2-} quickly recombines with S^{2-} to form S_8^{2-} again, which explains the coexistence of S_8^{2-} and S_7^{2-} at 16% of elapsed time. This recombination results in a more favorable reaction of S_8^{2-} to produce stable S_6^{2-} and S_2^{2-} species. At high Li currents, on the contrary, S_7^{2-} continues to react to form shorter polysulfides instead of recombining back to S_8^{2-}. S_6^{2-} is observed to split into two S_3^{2-} although they rapidly recover back to S_6^{2-}; S_4^{2-} is seen to do the same and split into two S_2^{2-} by the end of the simulation. (Figure 9b). However, there are also similarities between both reaction mechanisms at different Li currents. For example, there is a rapid formation of S^{2-} species and coexistence with large polysulfides such as S_6^{2-} for both specific currents. This confirms what was stated above regarding the high reactivity of the system and a reaction path not necessarily taking place according to the reported mechanisms. The path exhibiting fast S^{2-} formation is seen at different simulation conditions: in presence of high (stoichiometric) or low (half stoichiometric) amount of Li, highly or weakly influenced by low coordinated carbon at the pore edge, and at different rates of lithium addition.

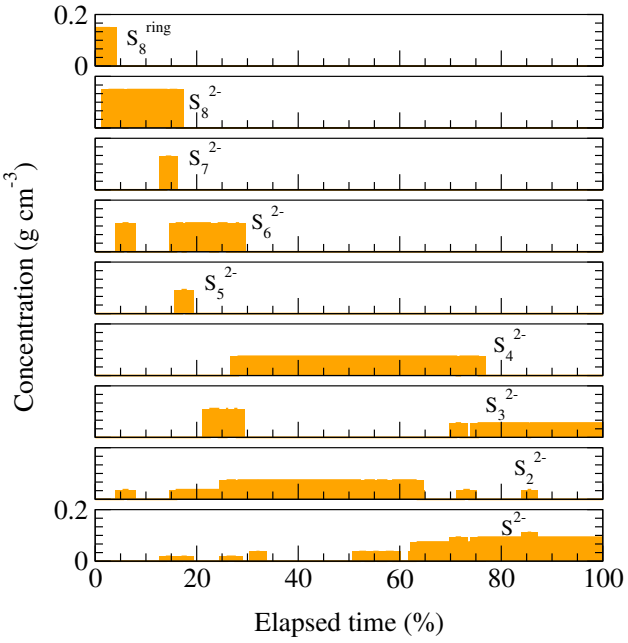

(a)

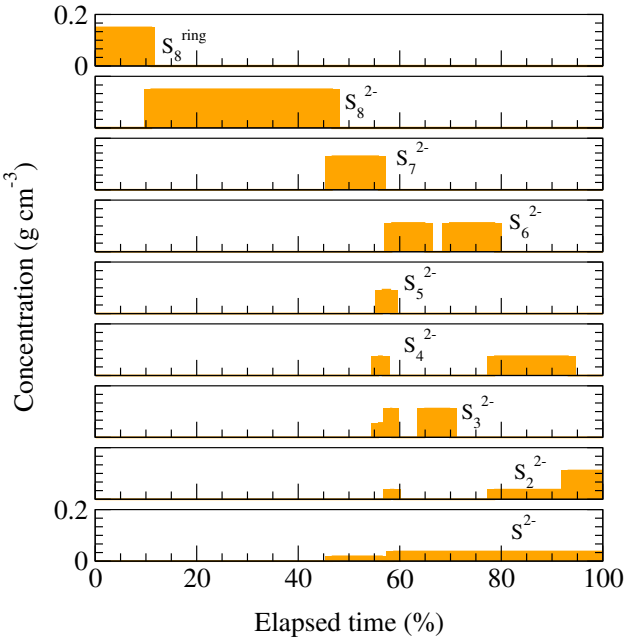

(b)

Figure 9: Concentration profile of polysulfide species along the AIMD trajectory for two different rates of Li addition into the system (a) 0.005 e^-/fs. (b) 0.020 e^-/fs. The concentrations correspond to the sum of anionic and molecular forms of an specific S_n species. All subfigures present the same range in the y-axis: between 0 and 0.2 g cm^{-3}.

Summary and Conclusions

Ab initio molecular dynamics (AIMD) simulations are used to analyze the physical-chemical behavior of sulfur/graphene systems that resembles C/S composite cathodes in Li-S batteries. The AIMD trajectories demonstrate a high reactivity and fast reduction of elemental sulfur to short polysulfide chains when Li ions are added to the system. The structure of the porous systems (separation between graphitic walls) may determine the reaction mechanisms and products obtained from the reduction. Polysulfide chains are trapped inside small carbon pores (1 nm) due to limited diffusion of long polysulfides in confined conditions and accumulation of Li ions outside the pore that prevented the relatively long polysulfide from reacting. DFT adsorption calculations demonstrate the strong interaction that exists between long polysulfides and graphitic surfaces of a small porous system. However, the absence of the solvent in this type of calculations invites to further investigate possible screening and diffusion effects exerted by the solvent molecules. The analysis of specific current confirms the reduction mechanisms showing high reactivity and rapid formation of short polysulfide chains from first S-S bond ruptures. It is observed that low specific currents favor the sulfur utilization via charge transfer, S-S bond breaking, and Li-S bond formation, which results in an improvement of the practical specific capacity.

Acknowledgement

This work was supported by the Assistant Secretary for Energy Efficiency and Renewable Energy, Office of Vehicle Technologies of the U.S. Department of Energy under Contract No. DE-EE0006832 under the Advanced Battery Materials Research (BMR) Program. Supercomputer resources from Texas A&M University High Performance Computer Center and Texas Advanced Computing Center (TACC) are gratefully acknowledged. Finally, J.A.M and J.C.B also thank the Vicerrectoría de Investigaciones of the Universidad de Cartagena for the support through internal research grants, and ANL's Center of Nanoscale Materials

for computational resources used to cross check and post-processing.

References

(1) Choi, N.-S.; Chen, Z.; Freunberger, S. A.; Ji, X.; Sun, Y.-K.; Amine, K.; Yushin, G.; Nazar, L. F.; Cho, J.; Bruce, P. G. Challenges Facing Lithium Batteries and Electrical Double-Layer Capacitors. *Angewandte Chemie International Edition* **2012**, *51*, 9994–10024.

(2) Thackeray, M. M.; Wolverton, C.; Isaacs, E. D. Electrical Energy Storage for Transportation–Approaching the Limits of, and Going Beyond, Lithium-ion Batteries. *Energy Environ. Sci.* **2012**, *5*, 7854–7863.

(3) Ji, X.; Nazar, L. F. Advances in Li-S Batteries. *J. Mater. Chem.* **2010**, *20*, 9821–9826.

(4) Yang, Y.; Zheng, G.; Cui, Y. Nanostructured Sulfur Cathodes. *Chem. Soc. Rev.* **2013**, *42*, 3018–3032.

(5) Bruce, P. G.; Freunberger, S. A.; Hardwick, L. J. Li-O_2 and Li-S Batteries with High Energy Storage. *Nat Mater* **2012**, *11*, 19–29.

(6) Yamin, H.; Peled, E. Electrochemistry of a Nonaqueous Lithium/Sulfur Cell. *Journal of Power Sources* **1983**, *9*, 281 – 287.

(7) Wang, J.; Yang, J.; Xie, J.; Xu, N.; Li, Y. Sulfur-Carbon Nano-Composite as Cathode for Rechargeable Lithium Battery Based on Gel Electrolyte. *Electrochemistry Communications* **2002**, *4*, 499 – 502.

(8) Ji, X.; Lee, K. T.; Nazar, L. F. A Highly Ordered Nanostructured Carbon-Sulphur Cathode for Lithium-Sulphur Batteries. *Nat Mater* **2009**, *8*, 500–506.

(9) Dreyer, D. R.; Park, S.; Bielawski, C. W.; Ruoff, R. S. The Chemistry of Graphene Oxide. *Chem. Soc. Rev.* **2010**, *39*, 228–240.

(10) Cao, Y.; Li, X.; Aksay, I. A.; Lemmon, J.; Nie, Z.; Yang, Z.; Liu, J. Sandwich-Type Functionalized Graphene Sheet-Sulfur Nanocomposite for Rechargeable Lithium Batteries. *Phys. Chem. Chem. Phys.* **2011**, *13*, 7660–7665.

(11) Ji, L.; Rao, M.; Zheng, H.; Zhang, L.; Li, Y.; Duan, W.; Guo, J.; Cairns, E. J.; Zhang, Y. Graphene Oxide as a Sulfur Immobilizer in High Performance Lithium/Sulfur Cells. *Journal of the American Chemical Society* **2011**, *133*, 18522–18525, PMID: 22017295.

(12) Wang, J.-Z.; Lu, L.; Choucair, M.; Stride, J. A.; Xu, X.; Liu, H.-K. Sulfur-Graphene Composite for Rechargeable Lithium Batteries. *Journal of Power Sources* **2011**, *196*, 7030 – 7034, 15th International Meeting on Lithium Batteries (IMLB).

(13) Chen, J.-j.; Zhang, Q.; Shi, Y.-n.; Qin, L.-l.; Cao, Y.; Zheng, M.-s.; Dong, Q.-f. A Hierarchical Architecture S/MWCNT Nanomicrosphere with Large Pores for Lithium Sulfur Batteries. *Phys. Chem. Chem. Phys.* **2012**, *14*, 5376–5382.

(14) Guo, J.; Xu, Y.; Wang, C. Sulfur-Impregnated Disordered Carbon Nanotubes Cathode for Lithium-Sulfur Batteries. *Nano Letters* **2011**, *11*, 4288–4294, PMID: 21928817.

(15) Demir-Cakan, R.; Morcrette, M.; Nouar, F.; Davoisne, C.; Devic, T.; Gonbeau, D.; Dominko, R.; Serre, C.; Frey, G.; Tarascon, J.-M. Cathode Composites for Li-S Batteries via the Use of Oxygenated Porous Architectures. *Journal of the American Chemical Society* **2011**, *133*, 16154–16160, PMID: 21882857.

(16) Xiao, L.; Cao, Y.; Xiao, J.; Schwenzer, B.; Engelhard, M. H.; Saraf, L. V.; Nie, Z.; Exarhos, G. J.; Liu, J. A Soft Approach to Encapsulate Sulfur: Polyaniline Nanotubes for Lithium-Sulfur Batteries with Long Cycle Life. *Advanced Materials* **2012**, *24*, 1176–1181.

(17) Yu, X.; Xie, J.; Li, Y.; Huang, H.; Lai, C.; Wang, K. Stable-Cycle and High-Capacity Conductive Sulfur-Containing Cathode Materials for Rechargeable Lithium Batteries.

Journal of Power Sources **2005**, *146*, 335 – 339, Selected papers pressented at the 12th International Meeting on Lithium Batteries12th International Meeting on Lithium Batteries.

(18) Dysart, A. D.; Burgos, J. C.; Mistry, A.; Chen, C.-F.; Liu, Z.; Hong, C. N.; Balbuena, P. B.; Mukherjee, P. P.; Pol, V. G. Towards Next Generation Lithium-Sulfur Batteries: Non-Conventional Carbon Compartments/Sulfur Electrodes and Multi-Scale Analysis. *Journal of The Electrochemical Society* **2016**, *163*, A730–A741.

(19) Kresse, G.; Hafner, J. *Ab initio* Molecular Dynamics for Liquid Metals. *Phys. Rev. B* **1993**, *47*, 558–561.

(20) Kresse, G.; Hafner, J. *Ab initio* Molecular-Dynamics Simulation of the Liquid-Metal–Amorphous-Semiconductor Transition in Germanium. *Phys. Rev. B* **1994**, *49*, 14251–14269.

(21) Kresse, G.; Furthmller, J. Efficiency of Ab-initio Total Energy Calculations for Metals and Semiconductors Using a Plane-Wave Basis Set. *Computational Materials Science* **1996**, *6*, 15 – 50.

(22) Kresse, G.; Furthmüller, J. Efficient Iterative Schemes for *Ab initio* Total-Energy Calculations Using a Plane-Wave Basis Set. *Phys. Rev. B* **1996**, *54*, 11169–11186.

(23) Born, M.; Oppenheimer, R. Zur Quantentheorie der Molekeln. *Annalen der Physik* **1927**, *389*, 457–484.

(24) Khne, T. D. Second Generation Car-Parrinello Molecular Dynamics. *Wiley Interdisciplinary Reviews: Computational Molecular Science* **2014**, *4*, 391–406.

(25) Perdew, J. P.; Burke, K.; Ernzerhof, M. Generalized Gradient Approximation Made Simple. *Phys. Rev. Lett.* **1996**, *77*, 3865–3868.

(26) Perdew, J. P.; Burke, K.; Ernzerhof, M. Generalized Gradient Approximation Made Simple [Phys. Rev. Lett. 77, 3865 (1996)]. *Phys. Rev. Lett.* **1997**, *78*, 1396–1396.

(27) Blöchl, P. E. Projector Augmented-Wave Method. *Phys. Rev. B* **1994**, *50*, 17953–17979.

(28) Kresse, G.; Joubert, D. From Ultrasoft Pseudopotentials to the Projector Augmented-Wave Method. *Phys. Rev. B* **1999**, *59*, 1758–1775.

(29) Parrinello, M.; Rahman, A. Crystal Structure and Pair Potentials: A Molecular-Dynamics Study. *Phys. Rev. Lett.* **1980**, *45*, 1196–1199.

(30) Parrinello, M.; Rahman, A. Polymorphic Transitions in Single Crystals: A New Molecular Dynamics Method. *Journal of Applied Physics* **1981**, *52*.

(31) Allen, M. P.; Tildesley, D. J. *Computer Simulation of Liquids*; Oxford university press, 1989.

(32) Schlick, T. *Molecular Modeling and Simulation: An Interdisciplinary Guide*; Springer Science & Business Media, 2010; Vol. 21.

(33) Monkhorst, H. J.; Pack, J. D. Special Points for Brillouin-Zone Integrations. *Phys. Rev. B* **1976**, *13*, 5188–5192.

(34) Ho, K.-M.; Fu, C.; Harmon, B.; Weber, W.; Hamann, D. Vibrational Frequencies and Structural Properties of Transition Metals via Total-Energy Calculations. *Physical Review Letters* **1982**, *49*, 673.

(35) Grimme, S.; Antony, J.; Ehrlich, S.; Krieg, H. A Consistent and Accurate Ab initio Parametrization of Density Functional Dispersion Correction (DFT-D) for the 94 Elements H-Pu. *The Journal of Chemical Physics* **2010**, *132*, 154104.

(36) Grimme, S.; Ehrlich, S.; Goerigk, L. Effect of the Damping Function in Dispersion Corrected Density Functional Theory. *Journal of Computational Chemistry* **2011**, *32*, 1456–1465.

(37) Su, Y.-S.; Fu, Y.; Cochell, T.; Manthiram, A. A Strategic Approach to Recharging Lithium-Sulphur Batteries for Long Cycle Life. *Nature Communications* **2013**, *4*.

(38) Barchasz, C.; Molton, F.; Duboc, C.; Leprêtre, J.-C.; Patoux, S.; Alloin, F. Lithium/Sulfur Cell Discharge Mechanism: An Original Approach for Intermediate Species Identification. *Analytical chemistry* **2012**, *84*, 3973–3980.

(39) Bader, R. F. W. A Quantum Theory of Molecular Structure and its Applications. *Chemical Reviews* **1991**, *91*, 893–928.

(40) Kamphaus, E. P.; Balbuena, P. B. Long-Chain Polysulfide Retention at the Cathode of Li–S Batteries. *The Journal of Physical Chemistry C* **2016**, *120*, 4296–4305.

Graphical TOC Entry